Molecular dynamics simulations of void and helium bubble stability in amorphous silicon during heavy-ion bombardment

Maria A. Okuniewski
Department of Nuclear, Plasma, and Radiological Engineering, University of Illinois, Urbana, Illinois 61801

Yinon Ashkenazy
Racah Institute of Physics, Hebrew University of Jerusalem, 91904 Jerusalem, Israel and Department of Materials Science and Engineering, University of Illinois, Urbana, Illinois 61801

Brent J. Heuser
Department of Nuclear, Plasma, and Radiological Engineering, University of Illinois, Urbana, Illinois 61801

Robert S. Averback
Department of Materials Science and Engineering, University of Illinois, Urbana, Illinois 61801

(Received 23 March 2004; accepted 19 July 2004)

A study of void and helium (He) bubble stability in amorphous silicon (*a*-Si) subjected to heavy-ion bombardment was conducted with molecular dynamics simulations. The effects of incident ion energy, incident ion direction, and He pressure were investigated. He bubbles with pressures equal to or greater than 0.1 kbar were found to be stable during isotropic 2 keV xenon (Xe) irradiation. Bubbles with pressures below this limit collapsed completely. On the other hand, voids and bubbles of all pressures were stable following *unidirectional* 2 keV Xe bombardment. In this case, the voids and bubbles became elongated and resisted closure, a phenomenon attributed to the inability of liquid Si to wet the flat, low-curvature internal surfaces of the open-volume defect. The void closure rates varied from 55 to 180 Å/dpa as the Xe projectile energy increased from 0.2 keV to 2 keV, respectively. An analytical model based on a viscous flow mechanism is presented to describe the behavior associated with the slowest closure rate. The faster rates are attributed to pressure-induced convective flow into the void. © *2004 American Institute of Physics*. [DOI: 10.1063/1.1791759]

I. INTRODUCTION

Irradiation of amorphous silicon (*a*-Si) is relevant to microelectronics applications, as well as serving as a prototypical tetrahedral, covalently bonded disordered solid. Molecular dynamics (MD) computer simulations offer a practical method to investigate such systems on an atomic scale. A few MD simulations have been conducted on irradiation of *a*-Si.[1–9] These studies focused on sputtering,[1,2] ion beam mixing,[3,4] ion beam induced amorphization and crystallization,[5,6] low-energy ion dopant effects on depth profiles,[7] and defect and pressure distribution in *a*-Si due to low energy Si bombardment.[8,9] Here we present MD simulations designed to study the effect of Xe bombardment on void and helium bubble stability.

Amorphous Si was chosen as a model system for the study of radioactive decay damage in nuclear waste glass. Within waste glass, α decay of actinides can lead to He accumulation. Bubbles, thought to contain He, have been observed in simulated waste glasses with a He concentration of 100 appm.[10] The He atomic density in bubbles within Si can reach values approaching 10^{23} cm^{-3} because of the weak He-He repulsive potential and high ($\approx$1 eV) enthalpy of solution.[11] The Xe ions used in this study resemble heavy recoils from actinide α-particle decay, which typically range from 70 to 100 keV.[10] The present study was limited to a maximum Xe energy of 2 keV, greater Xe energies would have required larger simulation cell sizes and much longer computation times.

II. SIMULATION PROCEDURES

The MD code Parallel Cascade (PARCAS) (Ref. 12) was specifically designed to simulate displacement cascades and was employed in this study. Approximately 30 Si interatomic potentials[13–16] and at least 11 methods to create *a*-Si exist.[17–27] The Stillinger and Weber (SW) potential[14] was chosen for Si-Si interactions and the melt-quench procedure was used to create an *a*-Si simulation cell. The SW potential and the melt-quench procedure produce very good agreement with the known *a*-Si structure factor obtained from diffraction data,[27,28] and result in a melting point reasonably close to that of *a*-Si ($T_m \sim 1050$ K).[27]

The starting point for the melt-quench procedure was a diamond lattice simulation cell with {100} faces containing 54 872 Si atoms, corresponding to $19\times19\times19$ unit cells with a *c*-Si lattice parameter of 5.43 Å.[29] Periodic boundary conditions were employed at all six faces of the cube. The temperature of this cell was raised to 3000 K, inducing liquid disorder, and equilibrated for 5 ps under a constant volume boundary condition. The system was then cooled at a rate of 0.005 K/fs via velocity scaling to 10 K, freezing in the liquidlike disorder. Finally, the system was relaxed under

a $P=0$ boundary condition at 10 K for 5 ps. A 20 Å diameter spherical void was created by removing Si atoms in the center of the simulation cell once the amorphous structure was obtained. The system was again allowed to relax after void introduction under the $P=0$ condition at 300 K for 20 ps, followed by cooling at a rate of 0.005 K/fs to 10 K. This relaxation step reduced the size of the void slightly to a diameter of ≈19 Å.

Bubbles containing He pressures of 0.01, 0.1, and 1.0 kbar were created within the *a*-Si simulation cell. The He number density within a bubble could be calculated using the Laplace equation ($P=2\gamma/r$) and the ideal gas law, but these equations become inaccurate for small radii and at high pressures.[30] The following procedure was therefore used to fill the void with He to create a bubble. First, a fcc He lattice was created using the Lennard-Jones potential for the He -He interaction with $\sigma=2.63$ Å and $\varepsilon=10.92$ K.[31] This cell, containing 2048 He atoms [$8\times8\times8$ unit cells with a lattice parameter of 4.24 Å (Ref. 29)], was heated to 500 K at constant volume for 5 ps with periodic boundary conditions. The system, now disordered, was then cooled at a rate of 0.01 K/fs to 10 K and held under constant volume conditions for 5 ps. This quenched in the gas phase. Finally, the system was relaxed for 30 ps under a constant pressure boundary condition that was set to the desired He bubble gas pressure. A 20 Å diameter sphere was removed from the center of the relaxed He system and inserted into the *a*-Si void. The corresponding number of He atoms within the bubble for pressures of 0.01, 0.1, and 1 kbar were 2l, 93, and 144, respectively. Notice the linearity associated with the ideal gas law does not predict the correct behavior of the He atomic density within the bubbles. The final *a*-Si He system was heated to 150 K for 500 fs, cooled at a rate of 0.005 K/fs to 10 K under a $P=0$ condition, then allowed to remain at 10 K for an additional 20 ps at $P=0$.

The purely repulsive Ziegler, Biersack, and Littmark (ZBL) potential[32] was used for He-Si interactions. A purely repulsive potential is justified by the low solubility of He in Si. For example, Raineri *et al.* found that the minimum concentration to form He bubbles in *c*-Si via implantation of 20 to 300 keV He ions was 3.5×10^{20} cm^{-3}, corresponding to a maximum He solubility of 0.007 [He]/[Si].[33] Such a low terminal solid solution solubility is consistent with the very limited chemical interaction of an inert gas within a solid. The primary interaction of He with the solid will be a volumetric dilatation associated with the elastic medium, an effect that truly is repulsive in nature. The purely repulsive potential reflects this interaction.

The ZBL potential was also used to describe Xe-Si and Xe-He interactions, as is typically done in simulations involving energetic collisions. The binary collision approximation associated with the ZBL potential is valid for these interactions because of the higher energies and because only a single Xe projectile (as opposed to a cluster of Xe atoms, for example) is introduced at a time. Xe projectiles with incident energies of 0.6, 1, and 2 keV were initiated at a distance of 40 Å from the center of the cube and directed toward the void/bubble. This was done to ensure that this void/bubble was within the displacement cascade region of each bombardment event. A typical 2 keV displacement cascade is shown in Fig. 1. This figure demonstrates that the displacement cascade is contained within the cell and that the displacement damage region reaches the void or bubble. The latter statement is not true for 0.2 keV events and a special procedure was used in this case, as described below.

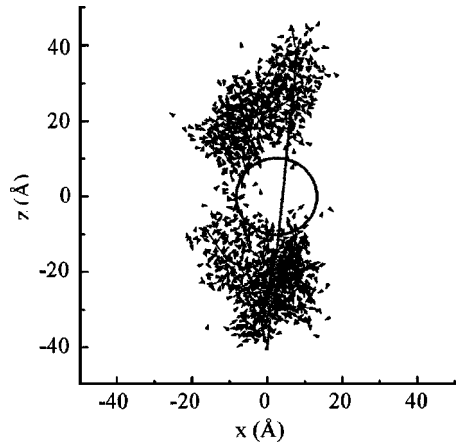

FIG. 1. Typical displacement cascade from a 2 keV Xe projectile near a 20 Å diameter void (represented by the circle). The projectile originated at $x=y=0$ and $z=-40$ Å. The center of the simulation cube and the center of the void are at $x=y=z=0$. The displacement cascade is shown after 30 ps have elapsed. Each arrow designates an atom which moved at least 1.0 Å and connects the starting and finishing position.

Xe was either introduced in a unidirectional manner (projectile initiated from the same location and direction for each event) or in an isotropic manner (projectile initiated at a random location for each event, but always at a radius of ≈40 Å and directed toward the void or bubble). The exception was the 0.2 keV Xe bombardment case, where both the initial direction and location of the projectile were chosen at random. Once a Xe projectile was introduced at $t=0$ with the cell at 10 K, the simulation continued for 30 ps at constant volume. This was sufficient for the displacement cascade to fully evolve with respect to time. Following this, a relaxation of the lattice was performed at $P=0$ for an additional 30 ps. Heat dissipation out of the simulation cell was facilitated by coupling the outer 10 Å of the cube to a 10 K temperature bath. One reason for directing the 0.6, 1, and 2 keV Xe projectiles toward the center of the cell was to ensure the displacement cascade did not occur within this heat sink boundary. The heat sink was also excluded from the volume available for introduction of the 0.2 keV projectiles. In all cases except the 0.2 keV set of simulations, the Xe projectiles were introduced sequentially, with the cell completely relaxed before initiation of the next event.

For the 0.2 keV events, the projectile was given both a random position and direction to allow the displacement cascades to encompass the majority of the *a*-Si volume. Eight 0.2 keV events were run simultaneously, one in each of the eight individual $42\times42\times42$ Å^3 cubes comprising the entire simulation cell volume without the heat sink boundary. This was done to accelerate the simulation and is justified since the range of a 0.2 keV Xe projectile is ≈20 Å. Although the direction and position of the 0.2 keV projectiles within each

TABLE I. Summary of simulation parameters.

Simulation Type	Xe Energy [keV]	He pressure [kbar]	Number of Events[a]	Number of Replicates[b]
Isotropic, variable energy	0.2	0.00	93	1
	0.6	0.00	20	1
	1.0	0.00	16	1
	2.0	0.00	10	1
Isotropic, variable pressure	2.0	0.00	10	1
	2.0	0.01	12	1
	2.0	0.10	14	1
	2.0	1.00	14	1
Unidirectional, variable pressure	2.0	0.00	5	4
	2.0	0.01	5	2
	2.0	0.10	5	3
	2.0	1.00	5	2

[a]Represents a single Xe bombardment event.
[b]Number of times entire sequence of events was repeated.

$42\times42\times42$ Å^3 cube was chosen randomly, projectiles directed toward the 10 Å heat sink boundaries were rejected before the simulation proceeded.

The volume of the void or bubble after each displacement-relaxation sequence was estimated with an algorithm designed to locate open regions in the simulation cell. This algorithm partitioned the entire simulation cell into $3\times3\times3$ Å^3 cubes. Each cube that did not contain a Si atom and also had at least three vacant (no Si atom present) nearest-neighbor cubes, contributed 27 Å^3 to the total void/bubble volume of the system. The outermost surface of the simulation cell was excluded from this algorithm so extraneous volume associated with the system boundaries was not included. It is important to note the total void/bubble volume calculated by this algorithm incorporated not only the void/bubble volume but also open volume associated with regions separate from the central void or bubble. The volume determined with this algorithm for the relaxed a-Si cell without a void or He bubble present was $\approx$200 Å^3. This value therefore represents the baseline open volume due to the disordered *a*-Si.

Three separate sets of simulations were performed to examine void and bubble stability: The effect of (i) incident Xe energy on void stability, (ii) He pressure on bubble stability, and (iii) incident Xe direction (isotropic versus unidirectional) on void and bubble stability. A summary of the simulation runs is provided in Table I.

III. RESULTS AND DISCUSSION

A. Void stability under isotropic bombardment

The effect of incident ion energy on void stability in *a*-Si under isotropic bombardment is presented first. The void volume versus simulation event number is shown in Fig. 2 for the four Xe energies investigated here. This figure demonstrates that an inverse relationship exists between the projectile energy and the number of events required to close or eliminate the void. In fact the number of events for complete void elimination (determined by visual inspection of the simulation cell after each event) scales well with inverse energy; 4, 9, and 16 events for 2, 1, and 0.6 keV respectively. This inverse scaling breaks down for the 0.2 keV case, where the expected number of events for closure would be $\approx$50. The void in the 0.2 keV case was still intact after 93 events, at which point the simulation sequence was terminated. The scaling behavior at higher projectile energies is, in fact, misleading; the analysis presented below demonstrates that the closure rate *on a displacement-per-atom* (dpa) *basis* does not depend as strongly on energy.

Another observation from Fig. 2 is the trend of larger residual open volume after void elimination as the projectile energy decreases. This could be a consequence of spontaneous annealing induced by the displacement cascades. Delaye and Ghaleb[34] noted annealing effects within nuclear waste glass subjected to different oxygen projectile energies. Through MD simulations, they discovered that annealing occurred more rapidly when sufficient recoil energy was available, which might explain the trend observed in our study. The residual volume for the low-energy cascades is dispersed throughout the entire simulation cell (original voids in the

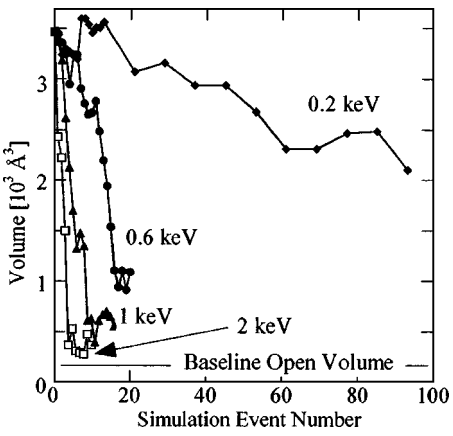

FIG. 2. Void volume vs simulation event number for the different Xe projectile energies studied under isotropic bombardment. The volume plotted in the figure was determined using an algorithm described in the text and represents both the volume associated with the original void and any additional vacancy defect clusters. The latter includes clusters that have broken away from primary void and clusters created during the displacement cascade independently of the primary void. The curves for the three highest energies level-off at the point where the void is completely eliminated. The baseline volume, $\approx$200 Å^3, is shown as the horizontal line and represents the open volume inherent to the as created *a*-Si.

center of the cell were completely eliminated) and is the result of small regions of free volume that persisted, perhaps because of insufficient annealing.

Analysis of the behavior shown in Fig. 2 begins by considering the void closure arising from radiation-induced viscous flow. An analytical expression for the void closure rate $\boldsymbol{v}_r$ can be derived by equating the energy dissipated via viscoelastic flow $\dot{W}$ and the time rate of change of the surface energy $\dot{E}_S$. The first term in this balance is given by the volume integral of the square of the stress tensor σ_{ij} of the viscous medium,[35]

$$\dot{W} = \frac{1}{2\eta}\int |\sigma_{ij}^2| dV, \tag{1}$$

where η is the viscosity. The stress tensor has the following diagonal elements in spherical coordinates:

$$\sigma_{rr} = 2\eta\frac{\partial v_r}{\partial r} = 2\eta\left(\frac{2R^2}{r^3}\right)v_o$$

$$\sigma_{\phi\phi} = 2\eta\frac{v_r}{r} = 2\eta\left(\frac{R^2}{r^3}\right)v_o$$

$$\sigma_{\theta\theta} = 2\eta\frac{v_r}{r} = 2\eta\left(\frac{R^2}{r^3}\right)v_o, \tag{2}$$

where R is the outer radius of the spherical medium and r is the inner or void radius. Eq. (2) assumes the medium is a viscous liquid that cannot support shear strains. The right-hand side of Eq. (2) was obtained using volume conservation during closure,

$$\frac{dr}{dt} = v_r = \frac{R^2}{r^2}\frac{dR}{dt} = \frac{R^2}{r^2}v_o, \tag{3}$$

where v_o is the rate at which the outer surface of the medium contracts. The integral given by Eq. (1) is evaluated as

$$\dot{W} = 16\eta v_o^2 R^4 \pi\left(\frac{1}{r^3} - \frac{1}{R^3}\right) \cong \frac{16\eta v_o^2 R^4 \pi}{r^3}, \tag{4}$$

where we assume $R^3 \gg r^3$.

The time rate of change of the surface energy is given by

$$\dot{E}_S = 8\pi R\gamma\frac{dR}{dt} + 8\pi r\gamma\frac{dr}{dt}$$

$$= 8\pi R\gamma v_o + 8\pi r\gamma\frac{R^2}{r^2}v_o \cong 8\pi\gamma\frac{R^2}{r}v_o, \tag{5}$$

where γ is the surface energy and Eq. (3) is used for the intermediate step. The required $\dot{W} = \dot{E}_S$ balance is given by equating Eqs. (4) and (5),

$$\frac{16\pi\eta v_o^2 R^4}{r^3} = 8\pi\gamma\frac{R^2}{r}v_o, \tag{6}$$

and, again using Eq. (3), it is found that

$$v_r = \frac{\gamma}{2\eta}. \tag{7}$$

TABLE II. Analysis of MD simulations of void closure for isotropic Xe projectile bombardment.

	0.2 keV	0.6 keV	1 keV	2 keV
Irradiated volume[a] [Å^3]	5.7×10^5	2.6×10^5	2.6×10^5	2.6×10^5
Si atoms[b]	2.9×10^4	1.3×10^4	1.3×10^4	1.3×10^4
Displacements per ion[c]	8	24	40	80
$d\phi/de$[c] [dpa]	2.8×10^{-4}	1.9×10^{-3}	3.1×10^{-3}	6.2×10^{-3}
dr/de[d] [Å]	0.015	0.15	0.43	1.1
$dr/de(d\phi/de)^{-1}$ [Å dpa]	55	80	140	180
$1/(\eta\dot{\phi})$[e] [(Pa dpa)$^{-1}$]	8.5×10^{-9}	1.2×10^{-8}	2.2×10^{-8}	2.8×10^{-8}

[a]Represents the volume of the simulation cell within which the projectiles were introduced. The outer boundary heat sink and the void are excluded from this volume for the 0.2 keV case. The volume for the 0.6, 1, and 2 keV cases also excludes the void and is defined by the 40 Å projectile-initiation radius (see text).
[b]Number of Si atoms within the irradiated volume.
[c]Displacements per ion using the modified Kinchin-Pease model, $0.8(E/2E_d)$ with E_d=10 eV, divided by the number of Si atoms.
[d]Slope of the data in Fig. 2 converted to dr/de using $r=(3V/4\pi)^{1/3}$, where V is the volume. This slope represents an averaged value from event zero (initial radius at $t=0$) to the event number where the curve leveled off or where the simulation was terminated (0.2 keV case).
[e]From Eq. (9) using a value of γ=1.3 N/m.

The slopes of the data in Fig. 2 are volumetric closure rates, but on a per-event basis. Conversion to a per-dpa basis is done by dividing by the dpa per incident Xe ion. The value of the dpa per Xe ion can be calculated using the modified Kinchin-Pease model. The closure rate is then given by

$$\frac{v_r}{\dot{\phi}} = \frac{dr}{dt}\left(\frac{d\phi}{dt}\right)^{-1} = \frac{dr}{de}\left(\frac{d\phi}{de}\right)^{-1}, \tag{8}$$

where $\dot{\phi}$ is in units of ions per second, dr/de is the closure rate, and $d\phi/de$ is the number of incident ions per event (equal to one by definition), but can also be written as dpa per event. Combining Eqs. (7) and (8), we have the following relationship for the closure rate on a per-dpa basis,

$$\frac{\gamma}{2\eta\dot{\phi}} = \frac{dr}{de}\left(\frac{d\phi}{de}\right)^{-1}. \tag{9}$$

Equation (9) allows a comparison of the results of the simulations (right-hand side) to an experimentally known quantity, the radiation-induced fluidity $1/(\eta\dot{\phi})$. The value of $1/(\eta\dot{\phi})$ has been determined by Mayr *et al.*[36] These authors found that a single, universal value of $1/(\eta\dot{\phi}) \sim 3\times10^{-9}$(Pa dpa)$^{-1}$ characterized the irradiation of amorphous solids (metallic glasses and glassy SiO_2). They also found that the same value characterized radiation-induced viscous flow in MD simulations of amorphous CuTi when the projectile energy exceeded 200 eV.[36]

The results of our simulations are shown in Table II. A systematic trend in the closure rate is observed, with the slowest rate at the lowest Xe projectile energy. We believe this trend signals a change in the closure mechanism from viscous flow at low projectile energy (as calculated above) to convective flow at high projectile energy. The latter mechanism is a consequence of the large momentum transfer within the displacement cascade directed toward the void. The ensuing pressure gradients force flow into the void open

volume, an effect not accounted for in the above viscoelastic model. Evidence of convective flow into the void during the MD simulations is presented in Sec. III C. It is reasonable that the lowest projectile energy simulated here gives the best agreement with work of Mayr *et al.*; the 0.2 keV cascades were initiated with a random location and direction, and the response of the *a*-Si medium is therefore closest to the viscous model. At the other extreme, the closure induced by convective flow overwhelms the viscous response and much higher rates (or fluidities) are observed for the 1 and 2 keV cases.

Values for the radiation induced fluidity obtained from our simulations are quoted in Table II. This calculation is based on Eq. (9) and required a value for the surface energy γ. We determined the surface energy for the *a*-Si lattice using MD and found $\gamma = 1.3$ N/m. This value is for a flat free *a*-Si surface at 70 K; the value determined from MD for the 20 Å void at 10 K is $\gamma = 1.1$ N/m. Both values compare well with crystalline (111) Si, $\gamma = 1.2$ N/m.[37]

The fluidity for the 0.2 keV case is approximately a factor of 3 higher than the universal value quoted by Mayr *et al.* This could be a consequence of several factors. For example, the SW potential may not adequately reproduce the elastic properties of *a*-Si. Alternatively, *a*-Si may behave differently from metallic glasses and SiO_2. It is also possible that the 0.2 keV case, such as the higher energy bombardments, is influenced by local melting when the displacement cascade is in the vicinity of the void.

The larger fluidities for the 1 and 2 keV cases are, in fact, a consequence of the internal free surface. In general, the radiation-induced fluidity of an amorphous solid is the response of the *infinite* medium to an applied stress during displacement damage. A free surface will perturb the response of an amorphous system, an effect investigated by Mayr *et al.* with MD.[36] These authors found that the fluidity did not level off with projectile energy to the above stated value, as it did for infinite geometry, but continually increased to $\approx 2 \times 10^{-8}$ (Pa dpa)$^{-1}$ at 10 keV.[36] Mayr *et al.* attributed this to mass flow onto the free surface caused by pressure within the cascades. Our higher energy results are thus consistent with this conclusion.

Finally, we mention the work of Zhu *et al.*, where nanocavity shrinkage was investigated in *a*-Si.[38] Voids with radii on the of order 100 Å were created in *c*-Si by hydrogen implantation followed by thermal annealing. The *c*-Si lattice in the vicinity of the voids was then amorphized by energetic (245 keV) Si irradiation. This same Si bombardment induced simultaneous shrinkage of the voids. Shrinkage as function of Si ion dose was quantified by Rutherford-backscattering (RBS) measurements of implanted Au getter efficiency. We estimated a void closure rate of ~ 20 Å/dpa from these measurements. The Kinchin-Pease model for dpa was used for this estimate. We also assumed that the measured Au getter efficiency is directly proportional to the radius of the void and that sufficient Au was present to saturate the trapping interaction prior to shrinkage. We also assumed that the initial cavity size quoted by Zhu *et al.* from TEM images is truly representative. Even though this estimate is significantly lower than our values in Table II still warrants presentation since it is the only experimental demonstration of cavity shrinkage in *a*-Si known to us.

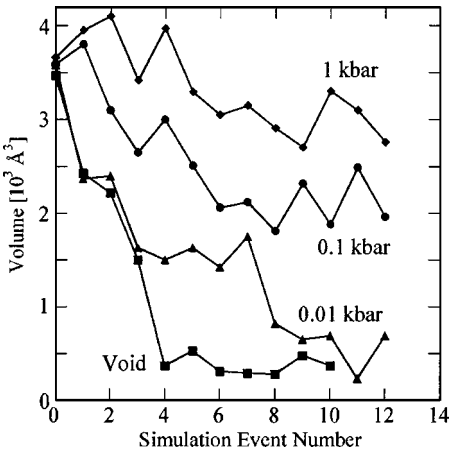

FIG. 3. Void (bubble) volume vs simulation event number during isotropic 2 keV Xe bombardment of cells containing He bubbles with the pressures shown. The slight variation in the initial bubble volume before Xe bombardment was due to the lattice relaxation following the introduction of He.

B. Isotropic, monoenergetic irradiations of He bubbles

The stability of He bubbles with pressures of 0.01, 0.1, and 1.0 kbar under isotropic 2 keV Xe bombardment was examined in the second set of simulations. The irradiation protocol was identical to that described for the high-energy cases in the preceding section. The bubble volume versus simulation event number is shown in Fig. 3. The 2 keV void simulation ($P = 0$) is shown for comparison. The two cases with highest bubble pressures did not close completely and therefore represent a stable defect. We believe this stabilizing effect is the result of the He gas pressure resisting displacement cascade-induced convective flow into the void. The 0.01 kbar bubble closed completely; bubbles with this pressure and lower are therefore not stable with respect to 2 keV Xe bombardment. Notice that the final volume for the 0.01 kbar case is equal to that of the void (≈ 500 Å^3), but is achieved after twice the number of simulated events.

The pressure required to stabilize a bubble, between 0.01 and 0.1 kbar, must be considered with the following caveat; the *a*-Si cell was initially at 10 K and the temperature spike within the first picosecond of the displacement cascade (not shown) significantly increased the pressure within the bubble, by perhaps a factor of 100. In other words, the same energy introduction that locally melted the *a*-Si simultaneously increased the He pressure, thereby enhancing the stability of the bubble at the given pressure. A greater He pressure would therefore be required to induce stability at a higher temperature.

While resisting closure, both the 0.1 and 1 kbar cases exhibited volume reductions. This is attributed to He emission shifting the balance point between internal gas pressure and flowing liquid penetration, causing the bubbles to restabilize at the new, smaller volume. He emission is the result of two effects, ballistic collisions, and the large pressure in-

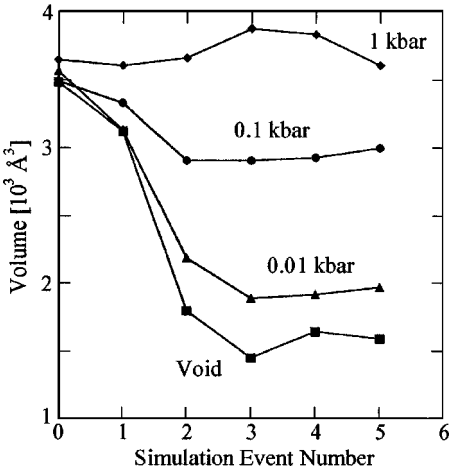

FIG. 4. Void (bubble) volume vs simulation event number during *unidirectional* 2 keV Xe bombardment of cells containing He bubbles with the pressures shown. These data represent averages obtained for the number of replicates listed in Table I.

crease associated with the above mentioned temperature spike. This effect would eventually lead to a complete loss of He from the bubbles and concomitant closure in the simulations. At a temperature where He atoms are mobile, however, a steady-state balance between He loss from the bubbles and He arrival to the bubbles (via diffusion) would be expected. The resulting He bubble distribution would then be at equilibrium with respect to the source strength of the alpha emitters embedded in the medium and with respect to heavy-ion bombardment from the recoil nuclei.

C. Unidirectional, monoenergetic irradiation

Lastly unidirectional irradiation of He bubbles with 2 keV Xe projectiles is considered. These results are shown in Fig. 4 and demonstrate that He bubbles of all pressures are stable with respect to unidirectional 2 keV Xe irradiation. Clearly, bubbles under these bombardment conditions are more stable than their isotropic counterparts. Even more noteworthy is that *voids* do not close completely and therefore exhibit a degree of stability not seen during isotropic irradiation.

The enhanced stability is a consequence of an elongated morphology that evolves under unidirectional bombardment. The elongated morphology evolves over the first three bombardment events; the lower pressure curves in Fig. 4 (void, 0.01, and 0.1 kbar) level off and therefore become stable after three events. The elongated morphology is evident in Fig. 5, which depicts the change in shape of a void during the first two simulated events. The extent to which a bubble elongated was inversely related to the internal He pressure; low-pressure bubbles elongated more than high-pressure bubbles (1 kbar bubbles exhibited slight elongation) and voids represented the most extreme case. Although the elongated morphology is interesting, it is strictly a consequence of the repeated introduction of Xe projectiles at the exact same "head-on" location and direction.

While the repeated head-on irradiation condition could never be achieved in a real experiment, the mechanism responsible for this elongation deserves discussion. Evidence

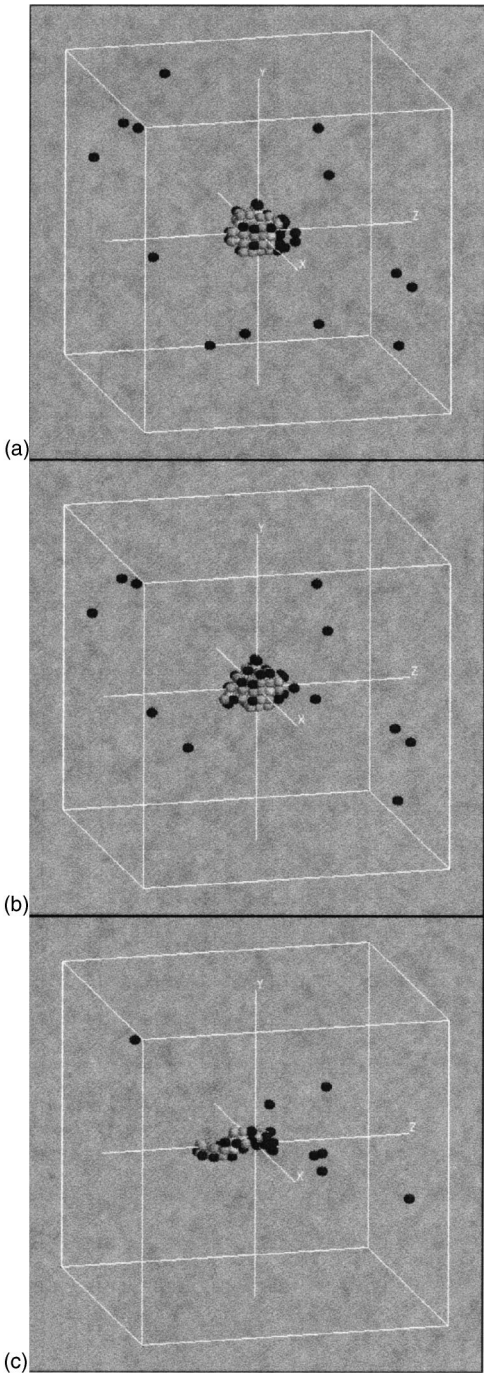

FIG. 5. Morphological evolution of a void during *unidirectional* 2 keV Xe bombardment: (a) before irradiation, (b) after the first event, and (c) after the second event. The projectiles were repeatedly introduced at the exact same location in the same direction and traveled from left to right along the *z* axis. The simulation cell is outlined in white.

of cascade-induced flow into the void is presented in Fig. 6. These snapshots, from the second simulated event shown in Fig. 5(c) demonstrate that localized melting within the displacement cascade causes Si atoms to flow into the void. As shown in Fig. 6, the flow coats the sides of the void nearest the point of introduction. This tends to elongate the void along the direction of Xe incidence, as best seen by the white-colored outlines in Fig. 6. The elongated morphology becomes very stable with respect to further introduction of liquid Si. We believe this is a consequence of the flat, low-

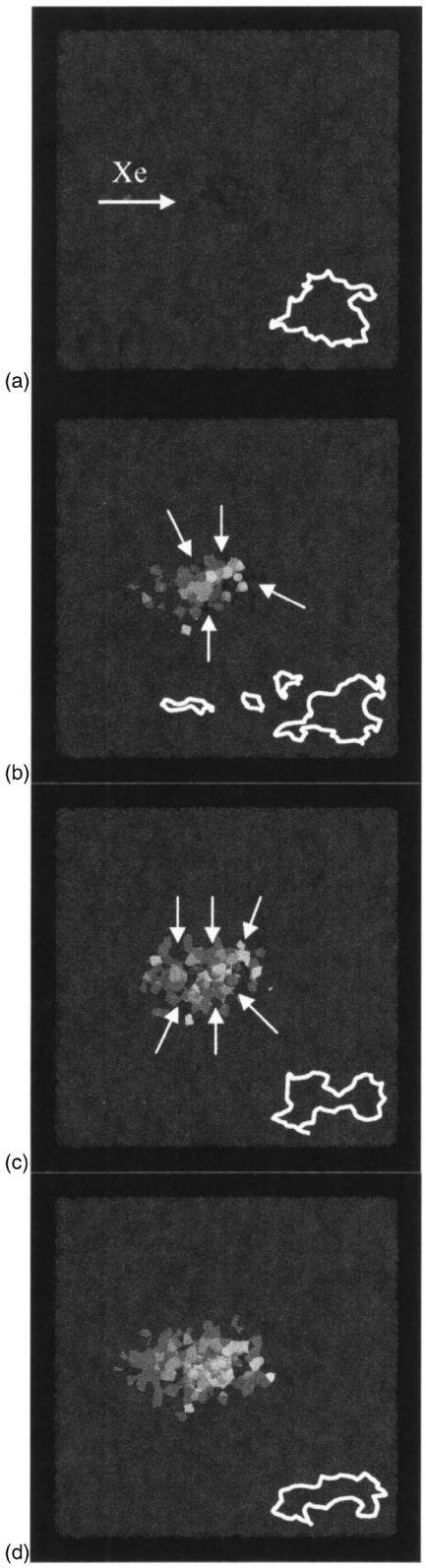

FIG. 6. Cross sectional views of the second 2 keV Xe bombardment event depicted in Fig. 5. The four frames correspond to (a) 0.025 ps, (b) 0.5 ps, (c) 2 ps, and (d) 60 ps. The views shown are cuts through the $y=0$ plane. The direction of Xe is shown in (a) as traveling from left to right. The white arrows point to Si atoms that have flowed into the void. The elongated morphology is best illustrated by the white outlines in the lower right hand corner of each slice. These outlines are traces of the open volume that have been shifted down and over for better illustration. Notice the three smaller vacancy clusters that develop at 0.5 ps and then disappear.

curvature void surfaces that develop along the direction of elongation. These surfaces resist further wetting by the liquid Si, thus stabilizing the elongated shape.

IV. CONCLUSIONS

Three primary conclusions can be made based on the MD simulations presented here.

(1) Voids in *a*-Si are unstable with respect to isotropic Xe bombardment. Although the number of events required for closure scaled inversely with energy, the closure rate *on a per-dpa basis* does not depend as strongly on energy. The void closure rates varied from 55 to 180 Å/dpa as the Xe projectile energy increased from 0.2 keV to 2 keV, respectively. We believe the slowest rate at 0.2 keV represents a viscous response of the medium, although the radiation-induced fluidity derived from this model is approximately a factor of 3 higher than the universal value quoted by Mayr *et al.* The faster rates at higher projectile energies are a consequence of convective flow into the void.
(2) He bubbles with gas pressures equal to or greater than 0.1 kbar are stable under isotropic 2 keV Xe bombardment at 10 K, while bubbles with pressures of 0.01 kbar or lower collapse completely. Presumably, bombardment with lower energy Xe projectiles would shift the stability point to lower He pressures. This was not investigated, however. The internal He pressure is thought to prevent penetration of liquid Si into the open volume during the displacement cascade. The temperature spike associated with the displacement cascade enhances this effect by temporarily increasing the He pressure within the bubble.
(3) Unidirectional irradiation induced an elongated void shape. The same elongated shape was observed during unidirectional bombardment of 0.01 kbar He bubbles, and, to a lesser extent, 0.1 kbar bubbles. The 1 kbar bubbles exhibited very little elongation. The elongated morphology was very stable with respect to closure under Xe bombardment. This is attributed to the inability of liquid Si to wet the flat, low-curvature surfaces along the length of the void or bubble.

ACKNOWLEDGMENTS

This work was supported by the Department of Energy, Nuclear Engineering Education Research (NEER) program under Grant No. DFG07-0l-ID14121 and in part by U.S. Department of Energy, Basic Energy Sciences under Grant No. DEFG02-91-ER45439. Computer simulations were carried out at the University of Illinois Materials Computation Center (MCC), a National Science Foundation Focus Research Group, under Grant No. NSF-DMR-9976550 and the National Center for Supercomputing Applications. The technical assistance of Greg Bauer, the MCC administrator, is greatly appreciated.

[1]J. E. Rubio, L. A. Marqués, M. Jaraíz, L. A. Bailón, and J. Barbolla, Nucl. Instrum. Methods Phys. Res. B **102**, 301 (1995).
[2]J. E. Rubio, L. A. Marqués, L. Pelaz, M. Jaraíz, and J. Barbolla, Nucl. Instrum. Methods Phys. Res. B **112**, 156 (1996).
[3]K. Nordlund and R. S. Averback, Appl. Phys. Lett. **70**, 3101 (1997).
[4]J. Tarus, K. Nordlund, J. Sillanpää, and J. Keinonen, Nucl. Instrum. Methods Phys. Res. B **153**, 378 (1999).
[5]B. Weber, D. M. Stock, K. Gäertner, and C. Wende, Radiat. Eff. Defects Solids **141**, 161 (1997).
[6]B. Weber, D. M. Stock, and K. Gäertner, Nucl. Instrum. Methods Phys. Res. B **148**, 375 (1999).
[7]Y. Yamamura, Nucl. Instrum. Methods Phys. Res. B **153**, 410 (1999).
[8]M. Koster and H. M. Urbassek, Nucl. Instrum. Methods Phys. Res. B **180**, 299 (2001).
[9]M. Koster and H. M. Urbassek, Surf. Sci. **496**, 196 (2002).
[10]W. J. Weber *et al.*, J. Mater. Res. **12**, 1946 (1997).
[11]G. F. Cerofolini, F. Corni, S. Frabboni, C. Nobili, G. Ottaviani, and R. Tonini, Mater. Sci. Eng., R. **27**, 1 (2000).
[12]PARCAS was written by K. Nordlund; see, for example, K. Nordlund, and R. S. Averback, Phys. Rev. B **56**, 2421 (1997).
[13]M. Schiable, Crit. Rev. Solid State Mater. Sci. **24**, 265 (1999).
[14]F. H. Stillinger and T. A. Weber, Phys. Rev. B **31**, 5262 (1985).
[15]R. Biswas and D. R. Hamann, Phys. Rev. Lett. **55**, 2001 (1985).
[16]J. Tersoff, Phys. Rev. B **39**, 5566 (1989).
[17]F. Wooten, K. Winer, and D. Weaire, Phys. Rev. Lett. **54**, 1392 (1985).
[18]D. E. Polk and D. S. Boudreaux, Phys. Rev. Lett. **31**, 92 (1973).
[19]M. D. Kluge, J. R. Ray, A. Rahman, Phys. Rev. B **36**, 4234 (1987).
[20]R. Biswas, G. S. Grest, and C. M. Soukoulis, Phys. Rev. B **36**, 7437 (1987).
[21]R. Car and M. Parinello, Phys. Rev. Lett. **60**, 204 (1988).
[22]P. C. Kelires and J. Tersoff, Phys. Rev. Lett. **61**, 562 (1998).
[23]D. A. Drabold, P. A. Fedders, O. F. Sankey, and J. D. Dow, Phys. Rev. B **42**, 5135 (1990).
[24]N. C. Cooper, C. M. Goringe, and D. R. Mckenzie, Comput. Mater. Sci. **17**, 1 (2000).
[25]M. Ishimaru, S. Munetoh, and T. Motooka, Phys. Rev. B **56**, 15133 (1997).
[26]W. D. Leudtke and U. Landman, Phys. Rev. B **37**, 4656 (1988).
[27]W. D. Leudtke and U. Landman, Phys. Rev. B **40**, 1164 (1989).
[28]M. D. Kluge, J. R. Ray, A. Rahman, Phys. Rev. B **36**, 4234 (1987).
[29]D. R. Lide, *CRC Handbook of Chemistry and Physics*, 76th ed. (CRC Inc., Boca Raton, Florida, 1995).
[30]S. E. Donnelly, Radiat. Eff. **90**, 1 (1985).
[31]R. A. Aziz, A. R. Janzen, and M. R. Moldover, Phys. Rev. Lett. **74**, 1586 (1995).
[32]J. F. Ziegler, J. P. Biersack, and U. Littmark, *The Stopping and Range of Ions in Solids* (Pergamon, New York, 1985).
[33]V. Raineri, P. G. Fallica, G. Percolla, A. Battaglia, M. Barbagallo, and S. U. Campisano, J. Appl. Phys. **78**, 3727 (1995).
[34]J. M. Delaye and D. Ghaleb, Nucl. Instrum. Methods Phys. Res. B **153**, 157 (1999).
[35]L. D. Landau and E. M. Lifshitz, *Fluid Mechanics* (Pergamon, New York, 1987).
[36]S. G. Mayr, Y. Ashkenazy, K. Albe, and R. S. Averback, Phys. Rev. Lett. **90**, 055505 (2003).
[37]Y.-M. Chiang, D. Birnie, and W. D. Kingery, *Physical Ceramics: Principles of Ceramic Science and Engineering* (John Wiley & Sons, Hoboken, 1997).
[38]X. F. Zhu, J. S. Williams, M. J. Conway, M. C. Ridgway, F. Fortuna, M.-O. Ruault, and H. Bernas, Appl. Phys. Lett. **79**, 3416 (2001).